Nickel ferrite nanoparticle as a magnetic catalyst: Synthesis and dye degradation

M. Kamel Attar Kar[a], F. Manteghi[a], M. Ghahari[b*]

[a]Department of Chemistry, Iran University of Science and Technology, Tehran, Iran
[b]Nanocoating and Nanomaterials Department, Institute for Color Science and Technology, Tehran, Iran

Abstract

The aim of this work is the synthesis of $NiFe_2O_4$ nanoparticles to catalyze photodegradation of direct red 264 under visible light. So, $NiFe_2O_4$ nanoparticles were synthesized by a sol-gel auto-combustion method. The catalyst was characterized by XRD, SEM, FT-IR and DRS.
The effect of $NiFe_2O_4$ nanoparticles as a catalyst was studied on photocatalytic degradation of Direct Red 264 (DR264) in typical wastewater using visible light irradiation. UV-vis spectrophotometer was used to measure concentration of dyes before and after degradation.

Keywords: Nickel nanoferrites; photocatalytic degradation; azo dyes.

1. Introduction

Environmental problem of toxic wastewater is one of the main subjects that researchers work on. Due to this, organic dyes are one of the main industrial wastewater pollutions. More than 50% of textile dyes is azoic dyes which are recognized by nitrogen π-bound. Textile and industrial dyes contain large groups of organic compounds that produce more than 7,000,000 ton per year. About 1–20% of world dye products enter into textile wastewater during the dyeing process [1].
Various physicochemical methods, such as adsorption on activated carbon, electrocoagulation, flocculation, froth flotation, ion exchange, membrane filtration, ozonation, and reverse osmosis, are used for the decolorization of dyes in wastewater. These methods are inefficient, expensive, have less applicability, and produce wastes in the form of sludge, which again needs to be disposed off. However, the degradation of azo dyes has gained considerable interest of researchers as it is inexpensive, eco-friendly, and produces less amount of sludge [2].
In spinel ferrites oxygen ions are in a fcc arrangement with the A ions in tetrahedral vacancies and B ions in octahedral vacancies. In normal spinel structure M^{2+} are in A sites and Fe^{3+} are in B sites but in inverse spinel structures M^{2+} are in B sites and Fe^{3+} are equally divided between A and B sites. The divalent and trivalent ions normally occupy the B sites in a random fashion. [3].
Spinel ferrites are an effective catalyst for oxidation and oxidative dehydrogenation reactions [4]. Processes that are environmentally benign, economical, efficient, and where the catalyst can be easily separated and recycled have become important in the chemical industry. Magnetic nanoparticles have some advantages, such as separation by magnetic properties. It is typically more effective than filtration or centrifugation because the loss of the catalyst is reduced. Magnetic separation is simple, economical and favorable for industrial applications [5]. $NiFe_2O_4$ has been chosen for their unique properties. Nickel ferrite has inverse spinel structure [6].
Various methods are used to synthesize ferrite nanoparticles, such as: combustion, mechano-chemical method, redox process, forced hydrolysis, co-precipitation, sol–gel, hydrothermal, polymer combustion method (PC), solid state method (SS), micro-emulsion, sonochemical, electrochemical and thermal decomposition method [7–15]. Among these, the combustion is one of the facile and one-step methods since it allows the preparation of nanocrystalline ferrites with an equiaxial shape, well-controlled morphology and narrow particle size distribution [16].

2. Experimental

2.1. Synthesis of $NiFe_2O_4$

The required amount of metal nitrates (nickel nitrate and iron nitrate) and citric acid are taken so as to have a molar ratio of 1:1 and dissolved in 100 ml of deionized water. A required amount of ammonia is added into the solution in order to modify the pH value to about 7. Dehydration of the solution was then done on a hotplate at 80◦C until a gel forms. Dry gels were heated in air to about 300◦C to invoke combustion. During combustion large amounts of gas were given off and a lightweight massive powder formed quickly. The resulting "precursor" powder was lightly ground by hand, as well as calcined at 850◦C for 2 h in a furnace to remove any organic rest [17, 18].

2.2 Photochemical reaction under visible light

Dye removal of Direct Red 264 was carried out by $NiFe_2O_4$ as a catalyst, H_2O_2 as an oxidant under visible lamp in the batch reactor. Sampling was carried out at various time intervals and the catalyst was adsorbed on to the external magnetic field. UV-Vis spectrophotometer was used to measure of concentration.

3. Results and discussion

3.1 XRD analysis

X-ray diffraction pattern of the sample is shown in Figure 1. The pattern indicates the formation of single-phase spinel ferrite by the conventional route. The XRD pattern was compared and indexed using ICDD card number (44–1485) for and $NiFe_2O_4$. The broad XRD line with small intensity indicates that the sample consists of ultrafine nanosized particles.

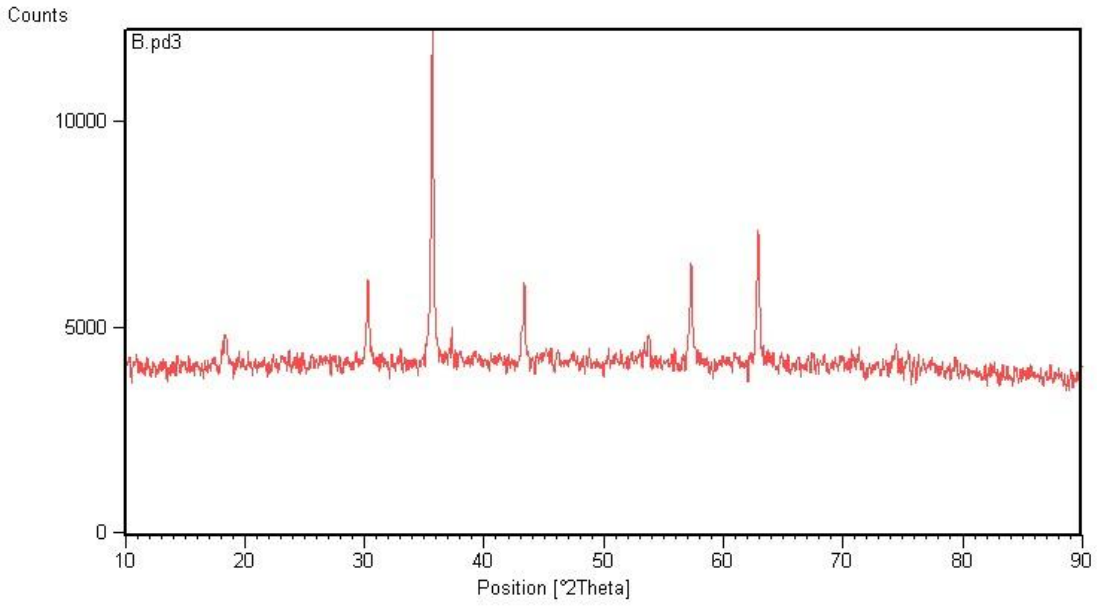

Fig.1 XRD pattern of $NiFe_2O_4$ nanoparticles.

3.2 FT-IR analysis

Figure 2 shows the FT-IR spectrum of the $NiFe_2O_4$ powders. The characteristic peaks of tetrahedral and octahedral complexes could be observed at 574 cm^{-1} and 416 cm^{-1}. It is clear that the normal mode of vibration of tetrahedral cluster is higher and normal mode of vibration of octahedral cluster is shorter. The tetrahedral cluster has shorter bond lengths and the octahedral cluster has longer bond lengths [19].

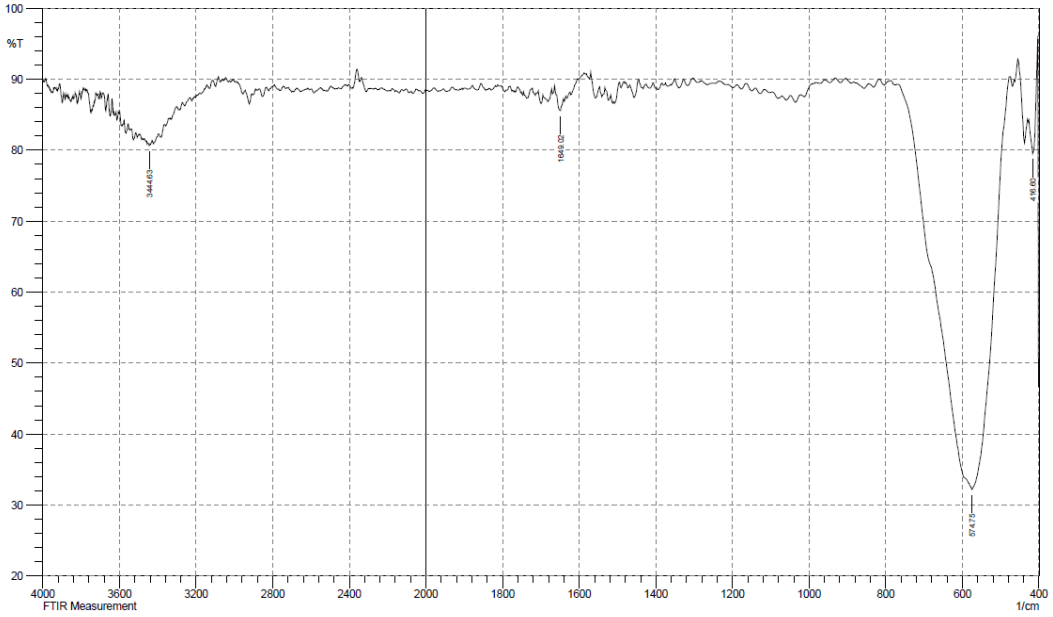

. **Fig.2** FT-IR spectrum of nanoparticles of $NiFe_2O_4$ nanopaticles.

3.3 SEM analysis

The micrograph of the single phase $NiFe_2O_4$ ferrite is taken with SEM as 21.00 KX magnifications (Fig. 3). It is clearly seen in the micrograph that the sample possess spherical nanosize grains. The average grain size determined from SEM was noted. In comparison with other samples, it was observed that the nanoparticles are single crystal, roughly spherical, uniformly distributed, but not highly agglomerated.

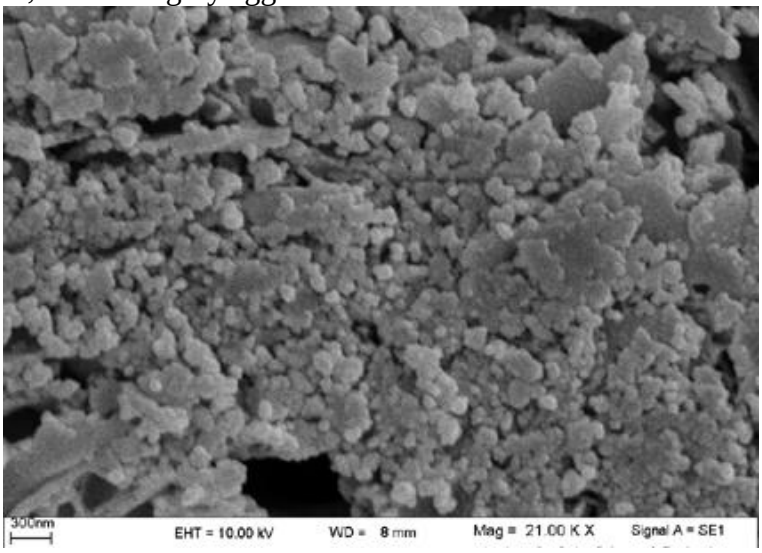

Fig.3 SEM image of $CuFe_2O_4$ nanopaticles.

3.4 DRS analysis

The analysis of optical absorption spectra is a powerful tool for understanding the band structure and band gap of both crystalline and noncrystalline materials. The optical properties of the ferrite samples were characterized by UV-DRS with the help of optical absorption data [20].Optical band gap of copper ferrite nanoparticles was estimated using the Kubelka-Munk relationship. The Kubelka–Munk plot $CuFe_2O_4$ has been presented in Figure 4. The calculated band-gap energy of $NiFe_2O_4$ was found to be 1.72 eV.

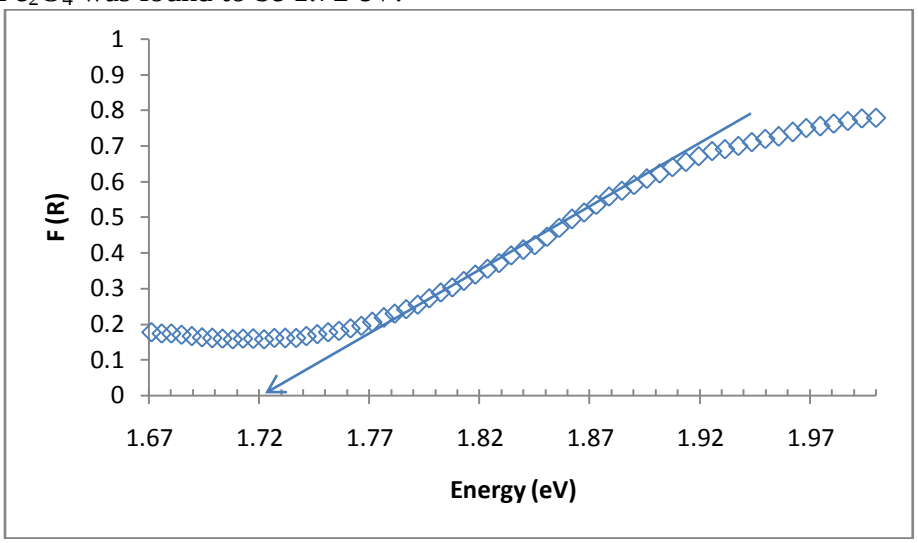

Fig.4 The Kubelka–Munk plot for $NiFe_2O_4$ nanopaticles.

3.5. Photocatalytic degradation

Dye degradation was estimated as follows:

$$Degradation = \frac{(A_0 - A_f)}{A_0} * 100 \quad (1)$$

Where A_0 is the initial and A_f is the final absorbance of the solution. Dye degradation of sample was calculated and following figure shows azo dye degradation plot for nanoferrites as a photocatalyst.

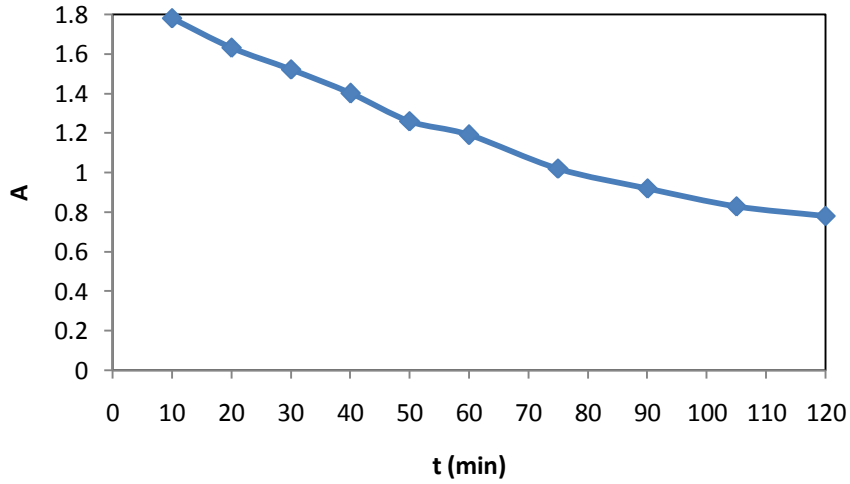

Fig.2 Photocatalytic degradation of DR 264 by $NiFe_2O_4$ nanopaticles as a catalyst.

4. Conclusion

$NiFe_2O_4$ nanoparticles have been successfully synthesized by sol-gel auto-combustion method. Band gap was calculated and to be 1.72 eV. It shows that it could be used as a catalyst. The samples have been successfully used as catalysts in photocatalytic degradation of DR 264 under visible irradiation.

References

[1] L. Karimi, S. Zohoori and M. E. Yazdanshenas, *Journal of Saudi Chemical Society*, 2014, **18**, 581–588.

[2] S. Lalnunhlimi and V. Krishnaswamy, *brazilian journal of microbiology*, 2016, **47**, 39–46.

[3] B. D. Cullity and C. D. Graham, *Introduction to magnetic materials*, IEEE Press (Wiley), United States of America, 2009, pp. 178–179.

[4] N. Ma, Y. Yue,W. Hua and Z. Gao, *Applied Catalysis A: General*, 2003, **251**, 39–47.

[5] T. Zeng, W. Chen, C.M. Cirtiu, A. Moores, G. Song and C.-J. Li, alkyne and amine, *Green Chemistry*, 12 (2010) 570– 573.

[6] S. Taghavi Fardood, A. Ramazani, Z. Golfar, S and W. Joo, 2017, DOI: 10.1002/aoc.3823.

[7] M.S. Khandekar, R.C. Kambale, J.Y. Patil, Y.D. Kolekar and S.S. Suryavanshi, *Journal of Alloys and Compounds*, 2011, **509**, 1861–1865.

[8] P. Kumar, S.K. Sharma, M. Knobel and M. Singh, *Journal of Alloys and Compounds*, 2011, **508**, 115–118.

[9] Y.-D. Xu, G. Wu, H.-L. Su, M. Shi, G.-Y. Yu and L. Wang, *Journal of Alloys and Compounds*, 2010, **12**, 112.

[10] J. Peng, M. Hojamberdiev, Y. Xu, B. Cao, J. Wang and H. Wu, *Journal of Magnetism and Magnetic Materials*, 2011, **323**, 133–138.

[11] P. Chandramohan, M. P. Srinivasan, S. Velmurugan and S. V. Narasimhan, *Journal of Solid State Chemistry*, 2011, **184**, 89–96.

[12] J. P. Vejpravova, V. Tyrpekl, S. Danis, D. Niznansky and V. Sechovsky, *Journal of Magnetism and Magnetic Materials*, 2010, **322**, 1872–1875.

[13] K. Kamal Senapati, C. Borgohain and P. Phukan, *Journal of Molecular Catalysis A: Chemical*, 2011, **1381**, 3–38.

[14] I. A. Amar, R. Lan, C.T.G. Petit, V. Arrighi and S. Tao, *Solid State Ionics*, 2011, **182**, 133–138.

[15] B. Y. Song, Y. Eom and T. G. Lee, *Applied Surface Science*, 2011, **257**, 4754–4759.

[16] M. S. Khandekara, R. C. Kambale, J. Y. Patil, Y. D. Kolekar and S. S. Suryavanshi, *Journal of Alloys and Compounds*, 2011, **509**, 1861–1865.

[17] A. Pradeep and G. Chandrasekaran, *Materials Letters*, 2006, 60, 371–374.

[18] N.J. Shirtcliffe, S. Thompson, E.S. O'Keefe, S. Appleton and C.C. Perry, *Materials Research Bulletin*, 2007, **42**, 281–287.